IEEE Access
Multidisciplinary | Rapid Review | Open Access Journal

Received 6 February 2024, accepted 6 March 2024, date of publication 19 March 2024, date of current version 25 March 2024.

Digital Object Identifier 10.1109/ACCESS.2024.3379149

RESEARCH ARTICLE

A Novel Lightweight Multi-Objective Optimization Design System for Vehicle Chassis Frames Based on ANFIS-SHAMODE-IWOA Model

ZHAO MINQING[1,2], WANG HONGXI[1], CHEN WEIHUAN[2,3], AND NING SHANPING[1,4]

[1]School of Mechanical and Electrical Engineering, Xi'an Technological University, Xi'an 710000, China
[2]JMC Automotive Product Research and Development Institute, Jiangling Motors Corporation Ltd., Nanchang 330000, China
[3]School of Information Engineering, East China Jiaotong University, Nanchang 330000, China
[4]School of Rail Transportation, Guangdong Communication Polytechnic, Guangzhou 330000, China

Corresponding author: Zhao Minqing (767432982@qq.com)

This work supported in part by the Research Program through the National Key Research and Development Program of China under Grant 2022YFB2503505; and in part by the Major Science and Technology Projects of Shaanxi Province, Xi'an, China, under Grant 2019zdzx01-02-02.

ABSTRACT In the process of daily product development and design, optimizing the shape and external dimensions of the vehicle chassis truss structure while considering both weight and reliability indicators often involves interdisciplinary collaboration and inefficient communication, leading to repetitive mechanical labor and low efficiency. This is widely regarded as a difficult and challenging task. In order to improve the design quality of the chassis truss structure and enhance work efficiency, this paper proposes a novel lightweight multi-objective optimization design system for vehicle chassis trusses based on the ANFIS-SHAMODE-IWOA model. Firstly, an adaptive spiral search strategy is introduced based on the multi-objective hybrid metaheuristic algorithm (SHAMODE) which is based on successful history. Then, a new SHAMODE-IWOA algorithm is proposed. In order to estimate the reliability level of the chassis truss structure under different design parameter combinations, a new ANFIS-SHAMODE-IWOA model is constructed by using the proposed SHAMODE-IWOA algorithm to learn the ANFIS model. Finally, in order to obtain the optimal design parameter combination, multi-objective optimization based on minimum design quality and optimal reliability measurement functions is studied using the SHAMODE-IWOA algorithm. Experimental results show that SHAMODE-IWOA has leading global optimization capability on CEC2017 test set benchmark functions. Compared with other intelligent models, the ANFIS-SHAMODE-IWOA model has better performance in reliability coefficient estimation. At the same time, the SHAMODE-IWOA algorithm obtains a more optimal design parameter combination for the chassis truss, with improvements of 9.5%, 12.5%, and 15% in Mass, Bending, and Torsion indicators, respectively. Ultimately, the proposed ANFIS-SHAMODE-IWOA multi-objective optimization design system, as a novel intelligent model, can be used to evaluate the reliability of chassis truss structures, improve development and design efficiency, and obtain the best design parameter combination, which is beneficial to improving the level of green intelligent manufacturing design.

INDEX TERMS Chassis truss, multi-objective optimization, ANFIS model, SHAMODE algorithm, lightweight, machine learning.

I. INTRODUCTION

The vehicle chassis is an important component that ensures the power output and smooth and reliable operation of the vehicle. The optimization design of the chassis is a key issue in vehicle lightweight optimization. During the process of lightweight optimization design, it is a challenging task for designers to consider both mass and reliability indicators while optimizing the shape and size of the chassis structure [1]. This often requires extensive finite element

The associate editor coordinating the review of this manuscript and approving it for publication was Jesus Felez.

simulation calculations and interdisciplinary collaboration to achieve satisfactory results. Currently, intelligent design and efficient high-quality design have become new trends in the manufacturing industry. Concurrently, the goal of design departments has become to create systems that enhance work efficiency and reduce interdepartmental coordination during interdisciplinary research. In the chassis design process, maintaining the reliable and durable performance of the chassis structure while reducing mass is a crucial factor in improving the design quality of the chassis structure, reducing vehicle energy consumption, and enhancing subsequent processing efficiency. Therefore, it is crucial to establish a lightweight auxiliary optimization design system that is computationally accurate, reliable in design, and efficient in computation.

Optimization algorithms are widely used in structural optimization work because of their ease of implementation, interpretability, and advantages in terms of robustness, adaptability, and code programming. In the early stages, genetic algorithm (GA) [2], [3] and simulated annealing(SA) [4] were the most commonly used optimization algorithms. Then, it entered the era of particle swarm optimization(PSO) [5] and differential evolution (DE) [6], where a large number of algorithms were subsequently developed and utilized. These include: grey wolf optimization algorithm [6], Symbiotic Organism Search Algorithm [7], cuckoo optimization algorithm [8], bat algorithm [9], hungry games search (HGS) algorithm [10], moth-flame optimization algorithm (MFO) [11], chaotic Levy flight distribution (CLFD) algorithm [12], cheetah optimization (CO) algorithm [13], and Henry gas solubility optimization algorithm (HGSO) [14] and so on.

In addition, optimization algorithms generally enable simultaneous search of multiple Pareto fronts in a single solving process, facilitating the resolution of multi-objective problems. However, their efficiency is lower and prone to local optima in handling high-dimensional problems or non-differentiable constraints [15], [16]. Therefore, in recent years, numerous novel and effective studies on multi-objective optimization problems of truss structures have been proposed. Aslan Busra and Yildiz Ali Riza applied lattice structure optimization method to optimize the structure of automobile suspension arms produced using additive manufacturing processes. The method was shown to obtain topologically optimized structures with higher reliability compared to other methods, although it has limitations when applied to non-additive manufacturing parts [17]. Kumar Sumit et al. proposed a decomposition-based multi-objective heat transfer search algorithm (MOHTS/D) to solve real-world structural problems. This algorithm can find optimal solutions with lower computational complexity and demonstrate better convergence, coverage, and diversity on the Pareto front. However, further investigation is needed to validate its performance in higher-dimensional and complex engineering design problems [18]. Mehta Pranav et al. proposed the use of the Hunger Games Search (HGS) algorithm for lightweight optimization of automobile suspension arms. This algorithm outperformed other algorithms in terms of performance. Nevertheless, its applicability and adaptability to other types of complex automotive components still need further investigation [19]. Kumar S. et al. aimed to improve the randomness and limitations of traditional metaheuristic algorithms in solving truss problems. They introduced the concept of dual archive (MOMVO2arc) based on the traditional multi-objective multi-verse optimizer (MOMVO). Comparative experiments showed that MOMVO2arc has higher efficiency in solving large-scale structural optimization problems. Yet, there is still room for further improvement and enhancement in this research [20]. Zhao Kaiwen et al. proposed an Adaptive Two-population Evolutionary Algorithm (ATEA) to address the difficulties in solving constrained multi-objective optimization problems. Extensive comparative experiments demonstrated the superiority of this algorithm. However, its adequacy in more complex real industrial scenarios lacks sufficient validation [21]. Pranav Mehta et al. proposed a novel gradient-based optimization algorithm (GBO) for structural optimization problems of heat exchangers and cooling towers. However, the research scope of this study needs to be further expanded [22]. Apiwat Nonut et al. introduced an L-SHADE algorithm for system identification of small fixed-wing UAVs. The algorithm exhibited good robustness and superior performance, but there is still room for further improvement in terms of solution performance [23].Natee Panagant et al. compared 18 different algorithms, including Successful History-based Adaptive Multi-objective Differential Evolution (SHAMODE), Successful History-based Adaptive Multi-objective Differential Evolution Without Archive (SHAMODE-WO), and Multi-Objective Iterative Parameter Distribution Estimation (MM-IPDE), in truss multi-objective optimization problems [24].

Based on the foundations, limitations, and inspirations from the mentioned studies, this paper presents a multi-objective optimization design system based on ANFIS-SHAMODE-IWOA. The system consists of three components:

Firstly, in response to the inadequate performance of the original algorithm, we have introduced an adaptive mechanism based on the SHAMODE-WO algorithm [24], and proposed the SHAMODE-IWOA algorithm. The improvement and effectiveness of this algorithm have been verified through benchmark function experiments.

Secondly, in order to estimate the reliability level of the chassis truss structure under different combinations of design parameters, the proposed SHAMODE-IWOA algorithm is used to learn the ANFIS.

Lastly, the SHAMODE-IWOA algorithm is applied to perform multi-objective optimization on the chassis truss in order to obtain the lowest quality and optimal reliability performance under different combinations of design parameters.

In summary, this study provides technical experience and theoretical basis for the lightweight and reliable design of

chassis truss structures. The design system has superior performance and can estimate reliability performance based on different combinations of design parameters. It can also obtain the optimal design parameter combination based on the lowest design quality and the best reliability performance. In addition, this system can reduce repeated finite element analysis and large-scale mechanical calculations in design activities, promote multi-disciplinary cooperation efficiency, enhance work efficiency while carrying out interdisciplinary cooperation, and reduce cross-department coordination processes, greatly improving design and production efficiency.

II. A NOVEL SHAMODE-IWOA ALGORITHM

The SHAMODE algorithm is an adaptive multi-objective differential evolution algorithm based on successful history. Its core idea is to utilize the historical information of individuals with superior objective function values to guide the mutation strategy of the differential evolution operator, thereby improving the algorithm's search capability [25]. The SHAMODE algorithm is derived from the SHADE algorithm and further solves multi-objective problems by updating the external Pareto archive [26]. The main steps of the SHAMODE algorithm include algorithm initialization, selection, mutation, crossover, and update.

To enhance the algorithm's search diversity and stimulate computational efficiency, this paper introduces an improved whale optimization algorithm (IWOA) with an adaptive spiral strategy into the original SHAMODE algorithm, and proposes a SHAMODE-IWOA algorithm. The specific steps of this algorithm are described as follows:

A. PARAMETER INITIALIZATION

NP initial solution sets are randomly generated, as shown in formula (1):

$$x_{i,G} = [x_{1,G}, x_{2,G}, x_{3,G}, \ldots, x_{NP,G}] \tag{1}$$

In formula (1), i is the index, NP is the index limit, equal to the number of design variables, and G is the iteration number.

Non-dominated solutions are populated in the initial Pareto archive Pareto1. At the same time, an empty external archive (A1) is created for the regeneration process. In this process, the initial values of all adaptive parameters are set. For more detailed information on adaptive parameters, please refer to sections II-E and II-F.

B. MUTATION

In the mutation process, a random strategy is adopted to generate a mutation term, as shown in formula (2):

$$u_{i,G} = x_{i,G} + V_{i,G}\left(x_{pbest} - x_{i,G}\right) + V_{i,G}\left(x_{r1,G} - \tilde{x}_{r2,G}\right) \tag{2}$$

In formula (2), $V_{i,G} \in [0,1]$ is a scaling factor that controls the influence of differential change. $x_{i,G}$ represents a feasible solution in generation G;x_{pbest} is a randomly selected solution from the external Pareto archive; $x_{r1,G}$ is a randomly selected solution from the current population (x_G), and $\tilde{x}_{r2,G}$ is a randomly selected solution from the union of the current population and the external archive. ($x_G \cup A_G$).

C. CROSSOVER

The crossover stage is performed according to the following formula (3):

$$h_{j,i,G} = \begin{cases} u_{j,i,G} \; if \; rand\,([0,1)) \le R_{i,G} or j = j_{rand} \\ x_{j,i,G} \; otherwise \end{cases} \tag{3}$$

In formula (3), $R_{i,G}$ represents the crossover ratio, with $R_{i,G} \in [0,1]$; $rand([0,1))$ denotes a uniformly distributed random number between 0 and 1;j_{rand} denotes the index of $\boldsymbol{x}$ randomly generated from [1,2,…, n], where $\boldsymbol{n}$ is the number of design variables.

D. CHOOSE

The joint population ($x_G \cup u_G$) consisting of the current individual $x_{i,G}$ and trial individual $h_{i,G}$ is sorted using the non-dominated sorting scheme of NSGA-II. The next iteration will retain NP solution candidates with the highest non-dominated level. If the number of solution candidates with the highest non-dominated level exceeds NP, some of them will be randomly removed to maintain a constant population size. Finally, the NP survivors of the current iteration are stored in x_{G+1}. After the selection process, all non-dominated solution candidates sorted from $h_G \cup Pareto_G$ are saved in $Pareto_{G+1}$. If the number of non-dominated solution candidates exceeds the maximum Pareto archive size, some will be randomly removed from the archive.

E. PARAMETER ADAPTIVE ADJUSTMENT STRATEGY

All adaptive parameters, including the external archive (A), the historical memory of the scaling factor (MF), and the crossover rate (MCR), are updated at the end of each iteration. Following the suggestion of L-SHADE [27], the maximum number of solutions in the external archive (A) is set to $1.4\times$ NP. At the end of each iteration, the indices of the successfully updated offspring that survived the selection process are stored in a vector called "$sind$". The parent vectors that generated the successful offspring (x_{sind}, G) are then stored in the external archive A_{G+1}. If the number of solutions stored in the external archive exceeds the specified value, some solutions are randomly deleted to maintain a constant archive size.

The updates for $V_{i,G}$ and $R_{i,G}$ are performed according to formula (4) and (5) as shown below:

$$V_{i,G} = randc_i(\mu_V, 0.1) \tag{4}$$

$$R_{i,G} = randn_i(\mu_R, 0.1) \tag{5}$$

In formula(4) and (5), μ_V and μ_R are the means, initially set to 0.5. $randc_i(\mu_V, 0.1)$ and $randn_i(\mu_R, 0.1)$ are random numbers generated based on Cauchy and Gaussian distributions, respectively, with variances (σ_V^2, σ_R^2) equal to (0.1, 0.1).

Furthermore, let M_V and M_R be the historical memory of the scaling factor $V_{i,G}$ and the crossover rate $R_{i,G}$, from which μ_V and μ_R for each individual can be randomly selected. At the end of each iteration, an element of the memory (MF and MCR) is updated using the Lehmer mean of the parameters of the successfully updated offspring, as described in formula (6) and (7):

$$M_{V,k,G+1} = \begin{cases} Lmean\left(V_{sind,G}\right) & if\ V_{sind,G} \notin \phi \\ M_{V,k,G} & otherwise \end{cases} \tag{6}$$

$$M_{R,k,G+1} = \begin{cases} Lmean\left(R_{sind,G}\right) & if\ R_{sind,G} \notin \phi \\ M_{R,k,G} & otherwise \end{cases} \tag{7}$$

In formula (6) and (7), $Lmean(V_{sind,G})$ and $Lmean(R_{sind,G})$ are the Lehmer means of $V_{i,G}$ and $R_{i,G}$, respectively, where sind denotes the individuals of the successful offspring. If at least one successful offspring exists, the $\boldsymbol{k}$-th memory position will be updated; otherwise, such elements remain unchanged. The index $\boldsymbol{k}$ is initially set to 1 and linearly increases with the progression of the process. If $\boldsymbol{k} >$ H, it is reset to 1.

F. IMPROVED ADAPTIVE SPIRAL STRATEGY OF WHALE OPTIMIZATION ALGORITHM(IWOA)

The spiral factor in the Whale Optimization Algorithm (WOA) has been shown in numerous studies to enhance the search diversity of the SHAMODE algorithm, where the WOA's spiral motion is integrated into the SHAMODE algorithm [6], [28]. During the mutation process, each mutation carrier $u_{i,G}$ has a chance to be further updated with the WOA's spiral motion, which is then activated during crossover, as described in formula (8) and (9) [29].

$$u_{i,G}^{\Theta} = \begin{cases} D_i e^{l} \cos\left(2\pi l\right) + x_{pbest2} & if\ rand < 0.5 \\ u_{i,G} & otherwise \end{cases} \tag{8}$$

$$D_i = \left|x_{pbest2} - u_{i,G}\right| \tag{9}$$

In formula (8) and (9), $u_{i,G}^{\Theta}$ is a new mutated variable with spiral update, and x_{pbest2} is another feasible solution randomly selected from the current Pareto archive (different from x_{pbest1}). The variables l and $rand$ are random numbers in the intervals $[-1, 1]$ and $[0, 1]$, respectively.

However, the setting of the l value determines that the spiral search phase can only follow a fixed spiral line, which leads to a too narrow optimization approach and increases the risk of premature convergence, weakening the global search capability of the algorithm. To address this issue, this paper introduces a variable that sets the spiral shape parameter l as a dynamic value that changes with the number of iterations, allowing whale individuals to dynamically adjust the spiral shape during the spiral search phase, enhancing the global search capability of the algorithm to improve its convergence accuracy. The improved strategy is shown in formula (10)(11)(12).

$$u_{i,G}^{\Theta} = \begin{cases} D_i e^{bl} \cos\left(2\pi l\right) + x_{pbest2} & if\ rand < 0.5 \\ u_{i,G} & otherwise \end{cases} \tag{10}$$

$$\mathrm{b} = -\gamma \sin\left(\frac{1}{2}\pi \sqrt{\frac{G_{max} - G}{G_{max}}}\right) \tag{11}$$

$$D_i = \left|x_{pbest2} - u_{i,G}\right| \tag{12}$$

In formula (10)(11)(12), γ is the spiral shape adjustment factor, G_{max} is the maximum number of iterations, and G is the current iteration number.

Thus, the pseudocode for the SHAMODE-iWOA algorithm is shown in Algorithm 1.

Algorithm 1 SHAMODE-IWOA

//Initialisation
Set population and maximum Pareto archive size to NP
Randomly generate initial population $x_{i,G} = [x_{1,G}, x_{2,G}, x_{3,G}, \ldots, x_{NP,G}]$
Select non-dominated solution from x_1 to be intial Pareto front(P),
Set maximum Pareto archive size to NP.
External Archive A $= \phi$, Set maximum external archive size to 1.4xNP
Set memory index k to 1, and memory size H to 5
Set all initial values in MF,MCR to 0.5
//Main loop
For G = 1 to G_{max} do
  // mutation operator
$V_{i,G} = \mathrm{randc}_i\left(\mu_V, 0.1\right)$
$u_{i,G} = x_{i,G} + V_{i,G}\left(x_{pbest} - x_{i,G}\right) + V_{i,G}\left(x_{r1,G} - \tilde{x}_{r2,G}\right)$
$u_{i,G}^{\Theta} = \begin{cases} D_i e^{bl} \cos(2\pi l) + x_{pbest2}\ if\ rand < 0.5 \\ u_{i,G}\ otherwise \end{cases}$
$\mathrm{b} = -\gamma \sin\left(\frac{1}{2}\pi \sqrt{\frac{Max_G - G}{Max_G}}\right)$
$R_{i,G} = \mathrm{randn}_i\left(\mu_R, 0.1\right)$
$h_{j,i,G} = \begin{cases} u_{j,i,G}\ if rand\ ([0, 1)) \le R_{i,G}\ \text{ or } j = j_{rand} \\ x_{j,i,G}\ otherwise \end{cases}$
$\boldsymbol{x}_{G+1}$ = best NP solution with highest non-dominated levels form $x_G \cup u_G$
Sind = set of indices of u_G that survived and are included in x_G
Pareto $_{G+1}$ = non-dominated solution from Pareto $G_G \cup u_G$
//Adaptive strategies
$AG + 1 = A_G \cup x_{sind,G}$
$M_{V,k,G+1} = \begin{cases} Lmean\left(V_{sind,G}\right)\ if\ V_{sind,G} \notin \phi \\ M_{V,k,G}\ otherwise \end{cases}$
$M_{R,k,G+1} = \begin{cases} Lmean\left(R_{sind,G}\right)\ if\ R_{sind,G} \notin \phi \\ M_{R,k,G}\ otherwise \end{cases}$
$\mathrm{k} = \begin{cases} k + 1 if\ k + 1 \le H \\ 1 otherwise \end{cases}$
maintain the maximum size of $\mathbf{Pareto}_{G+1}$ and $\mathbf{A}_{G+1}$ by randomly removing excess solutions
End for

III. A NOVEL ANFIS-SHAMODE-IWOA MODEL

The Adaptive Neuro-Fuzzy Inference System (ANFIS) is a complete system that combines neural networks and fuzzy systems, integrating the advantages of both fuzzy inference systems and neural networks. It is suitable for modeling and analysis of various highly complex nonlinear problems [30]. Its typical structure is shown in Figure 1 below, which is usually a five-layer neural network. The adaptive nodes in the square boxes are adjustable parameter sets within the nodes, while the fixed nodes in the circular boxes are fixed parameter sets.

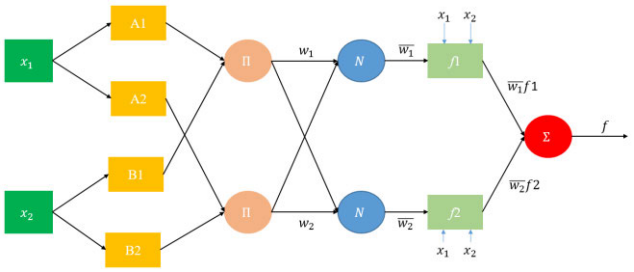

FIGURE 1. Schematic representation of the ANFIS infrastructure.

This paper is based on the SHAMODE-IWOA algorithm to learn the ANFIS model, with the aim of improving the efficiency and accuracy of the model. The specific steps for constructing the model are as follows:

Layer 1: This adaptive node is the membership function layer of the input variable, which converts the input into a fuzzy set, and the output function is:

$$Q_{1,i} = \mu_{A_i}(x_1) \quad i = 1, 2 \tag{13}$$

$$Q_{1,i} = \mu_{B_{i-2}}(x_2) \quad i = 1, 2 \tag{14}$$

In function (13) and (14), x_1 and x_2 are inputs; A_i and B_{i-2} represent fuzzy sets, i.e., linguistic variables obtained through calculation; μ_{A_i} and $\mu_{B_{i-2}}$ are membership functions, and the Gaussian function is used in this study:

$$\mu_i^j(x_i) = e^{\left(-\frac{(x_i - c_{ij})^2}{\sigma_{ij}^2}\right)} \tag{15}$$

In function (15), the parameters c_{ij} and σ_{ij} are initial parameters that need to be adjusted through the learning algorithm.

Layer 2: The function of this layer is to release the strength of the rules, and the node function is multiplied by the input to express the fuzzy rule:

$$Q_{2,i} = w_i = \mu_{A_i}(x_1) \cdot \mu_{B_{i-2}}(x_2) \tag{16}$$

Layer 3: The number of nodes is the same as that in the second layer, and the results of the previous step are normalized:

$$Q_{3,i} = \bar{w} = \frac{w_i}{w_1 + w_2} \tag{17}$$

Layer 4: This layer is the consequent network, which obtains the fuzzy if-then rules and calculates the output of the fuzzy rules:

$$Q_{4,i} = \bar{w}_i f_i = \bar{w}_i (p_i x_1 + q_i x_2 + r_i) \; i = 1, 2 \tag{18}$$

Layer 5: Output layer, calculating the total output of the input signal:

$$Q_{5,i} = \sum_i \bar{w}_i f_i \tag{19}$$

After the ANFIS model structure is established, the SHAMODE-IWOA algorithm is used to train the ANFIS

TABLE 1. Table of benchmark functions.

No	Funciton	Scope	Theoretical Optimum
1	Shifted and rotated bent cigar function	$[-100,100]^D$,D=20	100
2	Shifted and rotated bent cigar function	$[-100,100]^D$,D=20	200
3	Shifted and rotated zakharov function	$[-100,100]^D$,D=20	300
4	Shifted and rotated Rosenbrock's function	$[-100,100]^D$,D=20	400
5	Shifted and rotated Rastrigin's function	$[-100,100]^D$,D=20	500
6	Shifted and rotated expanded Scaffer's F6 function	$[-100,100]^D$,D=20	600
7	Shifted and rotated lunacek Bi_Rastrigin function	$[-100,100]^D$,D=20	700
8	Shifted and rotated non-continuous Rastrigin's function	$[-100,100]^D$,D=20	800
9	Shifted and rotated Levy function	$[-100,100]^D$,D=20	900
10	Shifted and rotated Schwefel's function	$[-100,100]^D$,D=20	1000
11	Hybrid Function 1 (N=3)	$[-100,100]^D$,D=20	1100
12	Hybrid Function 1 (N=3)	$[-100,100]^D$,D=20	1200
13	Hybrid Function 1 (N=3)	$[-100,100]^D$,D=20	1300
14	Hybrid Function 1 (N=3)	$[-100,100]^D$,D=20	1400
15	Hybrid Function 1 (N=3)	$[-100,100]^D$,D=20	1500
16	Hybrid Function 1 (N=3)	$[-100,100]^D$,D=20	1600
17	Hybrid Function 1 (N=3)	$[-100,100]^D$,D=20	1700
18	Hybrid Function 1 (N=3)	$[-100,100]^D$,D=20	1800
19	Hybrid Function 1 (N=3)	$[-100,100]^D$,D=20	1900
20	Hybrid Function 1 (N=3)	$[-100,100]^D$,D=20	2000
21	Composition Function 1 (N=3)	$[-100,100]^D$,D=20	2100
22	Composition Function 1 (N=3)	$[-100,100]^D$,D=20	2200
23	Composition Function 1 (N=3)	$[-100,100]^D$,D=20	2300
24	Composition Function 1 (N=3)	$[-100,100]^D$,D=20	2400
25	Composition Function 1 (N=3)	$[-100,100]^D$,D=20	2500
26	Composition Function 1 (N=3)	$[-100,100]^D$,D=20	2600
27	Composition Function 1 (N=3)	$[-100,100]^D$,D=20	2700
28	Composition Function 1 (N=3)	$[-100,100]^D$,D=20	2800
29	Composition Function 1 (N=3)	$[-100,100]^D$,D=20	2900
30	Composition Function 1 (N=3)	$[-100,100]^D$,D=20	3000

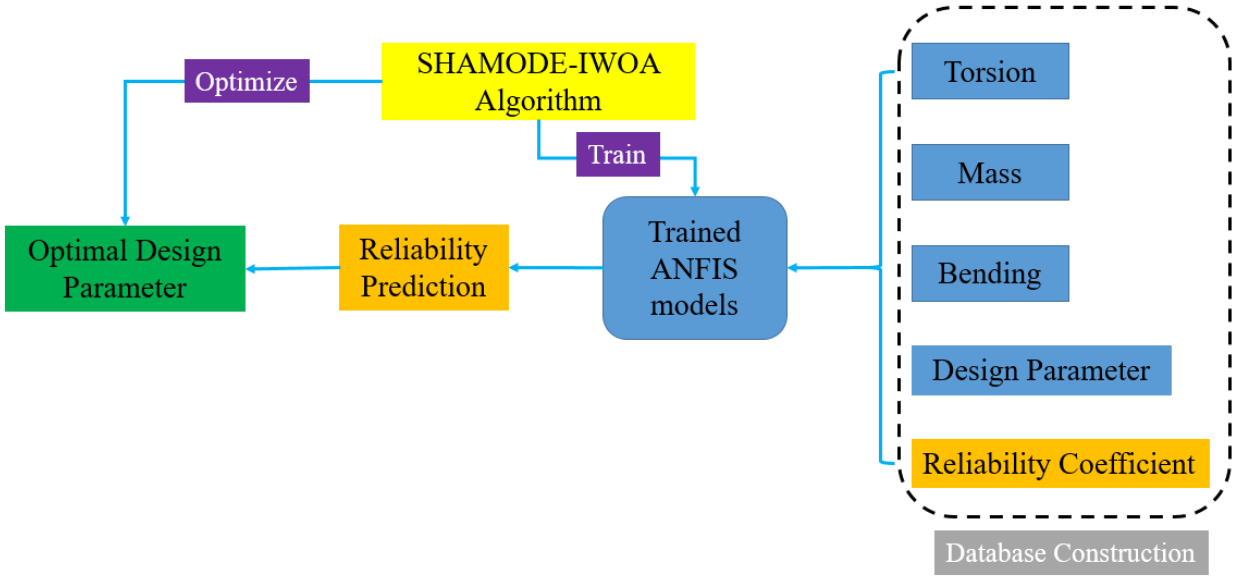

FIGURE 2. The overall work flow chart of the system.

model. The root mean square error (RMSE) is used as the fitness function to train the ANFIS, as follows:

$$\mathrm{RMSE} = \sqrt{\frac{\sum_{r=1}^{n} (d_r - p_r)^2}{n}} \tag{20}$$

In function (20), n is the number of training data in the training set; r is the r-th data, d_r is the actual value of the r-th training set data, and p_r is the r-th predicted value.

In this study, in order to obtain the best reliability and lowest quality design parameter combination, an ANFIS model was constructed with inputs such as Torsion, Mass, Bending, Design Parameter, and Reliability Coefficient, and the output is the reliability prediction result. In addition, the ANFIS model results were used as one of the objective functions to construct a multi-objective optimization model, ultimately obtaining the optimal design parameters. The overall work and model structure are shown in Figure 2.

IV. EXPERIMENTS AND RESULTS

A. TEST RESULTS OF SHAMODE-IWOA ALGORITHM

To verify the performance of SHAMODE-IWOA, this paper selects benchmark test functions from the CEC2017 test function set for testing. The function list is shown in Table 1, and the formulas in Table 1 are taken from reference [31]. Functions *f1-f3* are unimodal test functions, *f4-f10* are multimodal test functions, *f11-f20* are hybrid functions, and *f21-f30* are composition functions. The dimensionality (D) of the functions is set to 20. Different forms of test functions can be used to evaluate the optimization effectiveness and improvement of the algorithm. The results of the algorithm iterations are shown in Figure 3.

Based on the computational results obtained from Figure 3, the proposed SHAMODE-IWOA algorithm is compared with other optimization algorithms, including SHAMODE-WO [24], [28], Particle Swarm Optimization (PSO), Grey Wolf Optimization (GWO) [6], Whale Optimization Algorithm (WOA) [32], [33], African Vulture Optimization Algorithm (AVOA) [34], Gorilla Troop Optimization Algorithm (GTO) [35], Beetle Optimization Algorithm (DBO) [36], and Snake Optimization Algorithm (SO) [37]. The test results of the algorithms are presented in Table 2, where the first column represents the average values and the second column represents the standard deviations. The number of iterations is set to 500 [38].

Overall, the SHAMODE-IWOA algorithm achieves state-of-the-art solutions on 21 out of the total 30 test functions. This indicates that the improvement of SHAMODE-IWOA is effective within the CEC2017 test set, enabling the algorithm to obtain better solutions.

Specifically, for unimodal functions *f1-f3*, the SHAMODE-IWOA algorithm obtains the optimal solution among the compared algorithms for *f1* and *f2*, while it is slightly outperformed by the GTO algorithm for *f3*. This demonstrates that the SHAMODE-IWOA algorithm has certain advantages in terms of search capability for unimodal functions.

B. RELIABILITY ESTIMATION SYSTEM BASED ON ANFIS-SHAMODE-IWOA MODEL

Accurately predicting the structural fatigue life during the design and development stage is crucial. In order to enhance the flexibility of adding and removing design parameters in the lightweight design process, this section elaborates on the reliability estimation system of the ANFIS-SHAMODE-IWOA model.

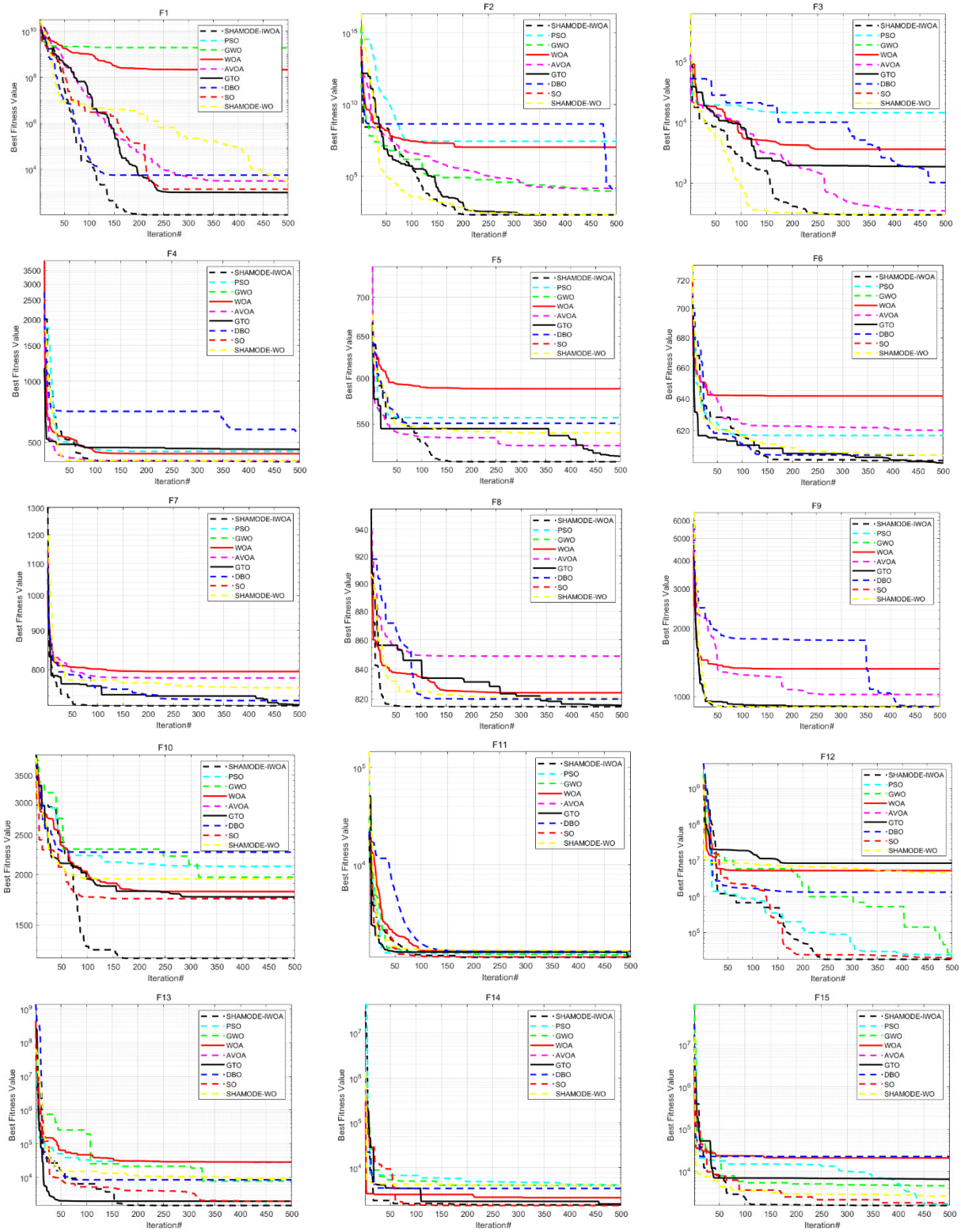

FIGURE 3. Comparison of the iterative calculation results of the algorithm.

1) ESTABLISHMENT OF THE DATABASE

As shown in the overall workflow diagram in Figure 2, it is necessary to construct the database required for the chassis truss structure research. The flowchart of the database construction process is illustrated in Figure 4.

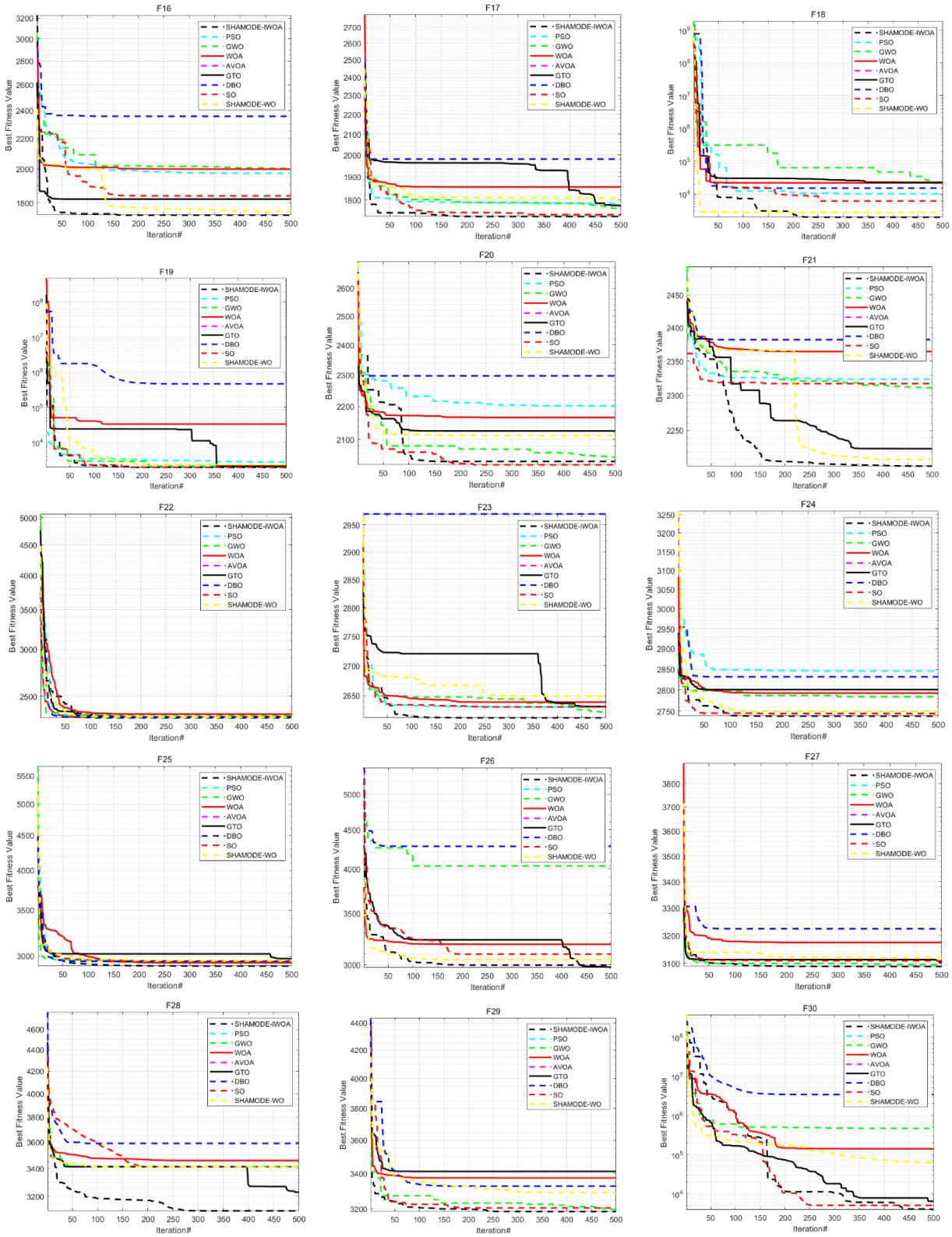

FIGURE 3. ***(Continued.)*** **Comparison of the iterative calculation results of the algorithm.**

First, the SFE model of the chassis truss structure is constructed as shown in Figure 5. The basic design parameters of the truss structure are shown in Table 3.

Then, after solving, the principal component analysis (PCA) method [39] is used to extract the design variables in the SFE model according to their

TABLE 2. Comparison table of function calculation results.

1	F1		F2		F3	
	Avg	Stdv	Avg	Stdv	Avg	Stdv
SHAMODE-IWOA	**2.0175E+03**	2.1963E+03	**6.4731E+10**	5.9143E+10	1.0574E+03	7.0924E+02
SHAMODE-WO	2.7092E+03	3.1982E+03	8.9024E+10	8.9014E+10	3.1346E+03	2.8197E+03
PSO	3.9756E+03	4.9231E+03	8.9724E+10	6.9724E+11	6.4174E+04	7.0145E+04
GWO	2.3172E+08	1.7847E+08	1.9756E+29	3.2864E+29	3.7164E+04	3.1724E+04
WOA	6.7159E+08	3.1758E+08	7.1563E+33	4.7154E+33	3.4791E+05	726162E+05
AVOA	5.4074E+07	4.7104E+06	7.5267E+26	6.9304E+26	1.2073E+05	3.1562E+05
GTO	2.1067E+06	1.7303E+06	1.9783E+34	2.3167E+34	**4.0754E+02**	2.3159E+02
DBO	6.9625E+07	4.7813E+07	3.8156E+19	3.1964E+19	4.8791E+04	3.1653E+04
SO	5.9762E+05	3.1075E+05	6.8921E+19	5.9413E+19	5.7604E+04	4.8714E+04
2	F4		F5		F6	
	Avg	Stdv	Avg	Stdv	Avg	Stdv
SHAMODE-IWOA	**2.3106E+02**	1.9435E+02	**3.9633E+02**	2.26791E+02	7.8761E+02	5.1362E+01
SHAMODE-WO	4.5025E+02	4.0141E+02	5.1125E+02	3.4157E+02	8.5168E+02	1.6326E+02
PSO	3.6794E+02	2.8714E+02	4.87601E+02	5.16275E+02	**6.8935E+02**	9.4013E+01
GWO	5.7146E+02	8.7142E+02	7.2145E+02	8.7912E+02	8.1423E+02	4.1679E+02
WOA	6.152E+02	7.6282E+02	6.8172E+02	6.1572E+02	8.9157E+02	7.1462E+02
AVOA	8.1503E+02	6.9753E+02	7.9934E+02	6.0931E+02	9.7618E+02	4.3319E+02
GTO	6.7145E+02	3.1573E+02	7.8903E+02	5.3178E+02	9.9023E+02	3.4703E+01
DBO	7.1467E+02	6.5314E+02	9.1435E+02	7.8146E+02	6.9014E+02	3.6702E+02
SO	5.4194E+02	4.3187E+02	8.7726E+02	7.9135E+02	2.3085E+03	3.7093E+00
3	F7		F8		F9	
	Avg	Stdv	Avg	Stdv	Avg	Stdv
SHAMODE-IWOA	**7.6903E+02**	5.9156E+02	9.9157E+02	2.7439E+02	**1.3475E+03**	7.8109E+02
SHAMODE-WO	8.1392E+02	4.6172E+02	9.4712E+02	3.1722E+02	3.1092E+03	1.2179E+02
PSO	8.9017E+02	7.0751E+02	9.6167E+02	3.9145E+02	3.7913E+03	1.8733E+03
GWO	7.6156E+03	5.6782E+02	9.4134E+02	2.5426E+02	2.45767E+03	1.7184E+03
WOA	5.6817E+03	6.7913E+02	9.8579E+02	3.1672E+02	3.7427E+03	4.5893E+03
AVOA	5.4173E+03	4.8914E+02	9.6186E+02	6.7921E+02	5.7012E+03	2.9157E+03
GTO	7.9315E+03	4.4143E+02	9.8732E+02	5.6791E+02	6.8215E+03	3.4175E+03
DBO	8.1406E+02	7.9146E+02	**8.3416E+02**	6.7081E+02	4.6154E+03	3.6742E+03
SO	6.9853E+03	4.5192E+02	8.9096E+02	7.0125E+02	5.1942E+03	3.0482E+03
4	F10		F11		F12	
	Avg	Stdv	Avg	Stdv	Avg	Stdv
SHAMODE-IWOA	**3.0513E+03**	1.9015E+02	**1.4692E+03**	4.8914E+01	**1.8064E+07**	2.0745E+06
SHAMODE-WO	5.1762E+03	3.1624E+02	2.1325E+03	2.8762E+02	3.4412E+07	3.0351E+06
PSO	4.7721E+03	2.9514E+02	1.6034E+03	1.7382E+02	2.3056E+07	3.0634E+06
GWO	5.6174E+03	2.1456E+02	2.4518E+03	8.1327E+02	8.1627E+07	6.1489E+07
WOA	7.0912E+03	8.1689E+02	7.1697E+03	3.5189E+02	3.4927E+07	9.6284E+07
AVOA	5.7146E+03	3.9154E+02	4.8764E+03	3.1451E+02	8.9144E+07	4.4912E+07
GTO	6.9874E+03	7.9013E+02	7.9013E+03	8.1659E+02	3.7892E+07	3.5891E+07
DBO	6.3163E+03	6.9147E+02	3.6913E+03	5.7694E+02	3.8914E+07	6.9813E+06
SO	7.0153E+03	4.0935E+02	3.0643E+03	4.9814E+02	4.0316E+07	7.8931E+06

TABLE 2. *(Continued.)* **Comparison table of function calculation results.**

5	F13		F14		F15	
	Avg	Stdv	Avg	Stdv	Avg	Stdv
SHAMODE-IWOA	**1.7206E+05**	5.7935E+04	2.1906E+03	5.1784E+04	**5.6071E+04**	2.0456E+02
SHAMODE-WO	2.9352E+05	7.8293E+04	2.9873E+03	4.6253E+04	8.7253E+04	3.3851E+02
PSO	1.9835E+05	8.4617E+05	3.8791E+03	4.8924E+03	7.8902E+04	4.5081E+02
GWO	1.1672E+07	2.1546E+06	2.9272E+05	3.1563E+05	3.7315E+05	7.2167E+03
WOA	8.9581E+06	5.8168E+06	2.6914E+06	2.5791E+06	5.0373E+05	6.1691E+04
AVOA	1.9058E+05	3.6781E+06	5.6157E+05	8.9158E+05	3.9514E+05	2.9051E+05
GTO	3.8052E+06	4.6926E+06	**1.7091E+03**	5.682E+04	8.7541E+05	9.0625E+05
DBO	4.7603E+06	5.7024E+06	6.8914E+03	4.1689E+03	9.0918E+04	7.0924E+04
SO	3.9784E+06	7.9268E+06	5.7184E+03	5.6982E+03	1.5629E+05	8.9034E+04
6	F16		F17		F18	
	Avg	Stdv	Avg	Stdv	Avg	Stdv
SHAMODE-IWOA	**2.1609E+02**	2.7108E+03	**2.1917E+03**	1.4261E+02	**3.0522E+04**	3.2172E+03
SHAMODE-WO	3.0782E+02	3.1642E+03	3.7025E+03	3.7421E+02	4.2763E+04	5.0125E+03
PSO	3.0187E+02	2.9842E+03	2.4057E+03	1.7514E+02	5.7781E+04	4.5162E+04
GWO	2.8156E+04	3.7257E+03	2.3346E+03	2.1517E+02	8.1589E+05	7.4163E+05
WOA	3.7914E+03	2.8713E+03	3.8727E+03	4.6272E+02	6.7925E+05	8.1592E+06
AVOA	5.6724E+04	4.0135E+04	5.613E+03	4.1613E+02	3.7983E+05	4.7781E+06
GTO	4.0463E+03	3.6792E+03	4.6182E+03	5.9513E+02	7.7734E+05	7.9903E+06
DBO	7.9084E+03	3.0413E+03	4.6013E+03	3.2103E+02	4.9143E+05	1.1523E+06
SO	1.0842E+04	5.7024E+04	5.1832E+03	2.7745E+02	5.6711E+05	4.5187E+05
7	F19		F20		F21	
	Avg	Stdv	Avg	Stdv	Avg	Stdv
SHAMODE-IWOA	**2.1335E+04**	1.6143E+03	**1.9732E+03**	1.7923E+02	**1.9023E+03**	1.9821E+01
SHAMODE-WO	3.4527E+04	3.1092E+03	2.9456E+03	2.3362E+02	3.0465E+03	3.0142E+01
PSO	5.9821E+04	2.8945E+03	3.1772E+03	1.6036E+02	2.7932E+03	2.5621E+02
GWO	3.1567E+05	6.1584E+05	3.1647E+03	1.6537E+02	6.8848E+03	4.1579E+02
WOA	5.7924E+06	4.6274E+06	5.1692E+03	2.6892E+02	7.5281E+03	1.7426E+01
AVOA	7.5142E+04	1.8075E+03	6.7192E+03	3.8153E+02	7.9024E+03	3.1042E+02
GTO	6.7724E+06	5.8724E+06	4.2731E+03	4.7193E+02	8.9024E+03	3.6891E+01
DBO	3.8719E+04	1.9215E+03	7.8142E+03	4.7745E+02	4.9824E+04	3.9023E+02
SO	4.8621E+04	2.6254E+03	6.9143E+03	3.2195E+02	5.0145E+03	2.0313E+02
8	F22		F23		F24	
	Avg	Stdv	Avg	Stdv	Avg	Stdv
SHAMODE-IWOA	3.1903E+03	2.4413E+03	3.1913E+03	4.9152E+01	**2.8156E+03**	2.9817E+01
SHAMODE-WO	3.7528E+03	3.4092E+03	3.2142E+03	4.7242E+01	3.4463E+03	3.1472E+01
PSO	2.9199E+03	2.9721E+03	2.9174E+03	3.9174E+01	4.4617E+03	3.4179E+01
GWO	4.2145E+03	3.1562E+03	2.8578E+03	3.726E+02	3.8153E+03	6.1536E+01
WOA	6.1573E+03	2.6153E+03	4.6892E+03	5.7189E+02	5.1792E+03	9.8373E+01
AVOA	**2.7902E+03**	2.3817E+03	5.4124E+03	3.4609E+01	5.6013E+03	4.0913E+01
GTO	4.5143E+03	3.0752E+03	3.8934E+03	5.7892E+02	6.7093E+03	6.0725E+01
DBO	4.7162E+03	2.9813E+03	3.9062E+03	5.7192E+01	4.5901E+03	4.8172E+01
SO	5.6181E+03	2.7513E+03	**2.1904E+03**	2.1614E+01	4.1461E+03	4.8031E+01

TABLE 2. *(Continued.)* Comparison table of function calculation results.

9	F25		F26		F27	
	Avg	Stdv	Avg	Stdv	Avg	Stdv
SHAMODE-IWOA	2.8893E+03	3.6179E+01	**3.9814E+03**	7.8921E+02	**2.9801E+03**	1.0153E+01
SHAMODE-WO	3.1431E+03	3.3053E+01	4.2621E+03	9.4273E+02	3.5182E+03	1.9341E+01
PSO	**2.8875E+03**	7.9142E+00	5.1421E+03	3.9195E+03	3.1032E+03	2.4151E+01
GWO	4.1352E+03	2.1673E+01	4.1497E+03	1.4824E+03	4.1529E+03	1.9153E+01
WOA	4.4714E+03	3.5582E+01	8.0215E+03	1.9728E+03	3.9942E+03	9.8726E+01
AVOA	3.7813E+03	4.1124E+01	5.0124E+03	2.7985E+03	3.7132E+03	5.9146E+01
GTO	4.4025E+03	3.6025E+01	5.6903E+03	3.5321E+03	4.5172E+03	6.4502E+02
DBO	4.7813E+03	3.1241E+01	4.9142E+03	3.1371E+03	5.0172E+03	7.0913E+01
SO	4.6099E+03	3.9143E+01	5.0191E+03	3.0152E+03	5.5242E+03	6.9021E+01
10	F28		F29		F30	
	Avg	Stdv	Avg	Stdv	Avg	Stdv
SHAMODE-IWOA	4.0913E+03	3.1903E+01	**3.3914E+03**	1.2517E+02	2.13418E+05	8.0921E+04
SHAMODE-WO	4.5793E+03	2.3142E+01	3.5921E+03	2.1093E+02	2.2195E+05	8.1462E+04
PSO	4.1315E+03	2.9702E+01	3.8061E+03	1.3146E+02	**1.97065E+05**	8.7042E+04
GWO	4.6913E+03	4.1928E+02	4.6157E+03	1.7924E+02	7.1527E+05	6.1592E+05
WOA	5.6681E+03	7.9158E+02	4.8158E+03	3.0891E+02	4.4603E+07	8.09156E+06
AVOA	**3.1091E+03**	2.9983E+01	4.1467E+03	3.1942E+02	8.9157E+07	2.1485E+07
GTO	5.7032E+03	6.9831E+02	5.4162E+03	4.6709E+02	9.1832E+07	7.9236E+05
DBO	6.0814E+03	4.0312E+01	4.08975E+03	3.9112E+03	6.9057E+06	3.1056E+05
SO	4.9362E+03	4.1312E+01	5.1147E+03	4.0121E+03	7.0814E+07	3.6193E+05

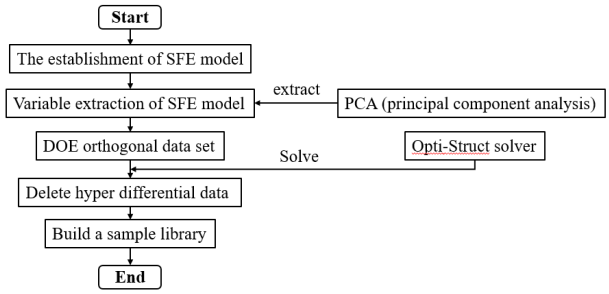

FIGURE 4. Schematic of the database construction.

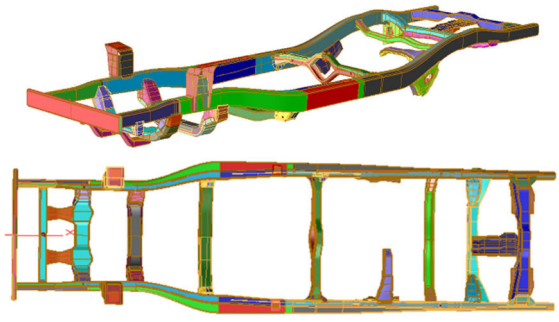

FIGURE 5. SFE model of chassis truss structure.

contribution levels, and the extraction results are shown in Figure 6.

TABLE 3. Table of SFE model parameters.

No	Parameter	Value
1	The X coordinates of the center of gravity	2478.8mm
2	The Y coordinates of the center of gravity	-1.9mm
3	The Z coordinates of the center of gravity	548.3mm
4	The principal inertia of the center of gravity I_X	37.3Kg.m^2
5	The principal inertia of the center of gravity I_Y	282.6Kg.m^2
6	The principal inertia of the center of gravity I_Z	319Kg. m^2
7	Torsion	212kN.m/rad
8	Bending	4312N/mm
9	First Twist Mode	28Hz
10	Mass	191.7Kg

The design variables with higher contribution levels are selected as design parameters. The list of design parameters and constraint ranges is shown in Table 4.

After generating the DOE matrix for the design variables in Table 4, the solutions for Bending, Torion, and Mass are calculated by a finite element solver, and the reliability index calculation method will be elaborated in Section VI. After excluding the abnormal data, the dataset shown in Table 5 is obtained.

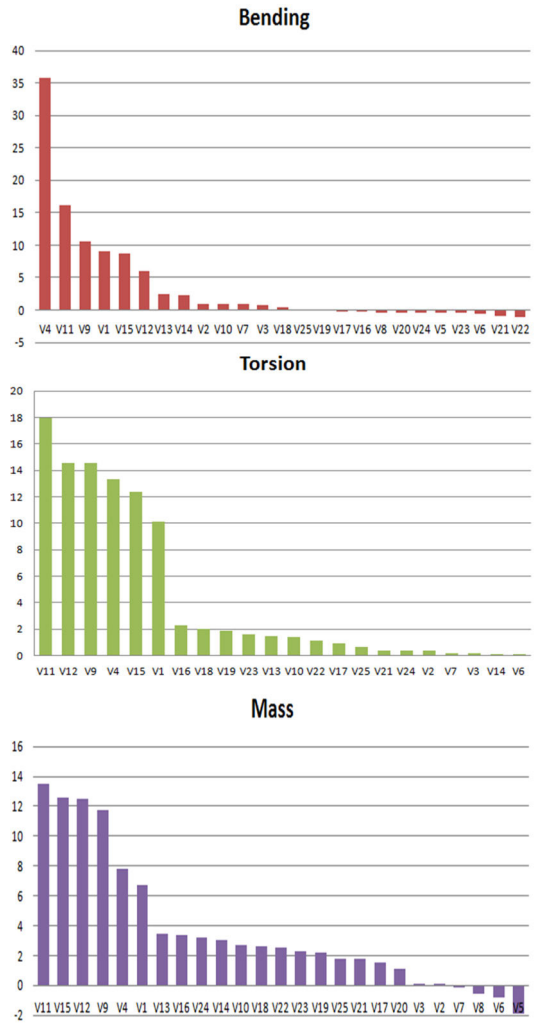

FIGURE 6. Principal component analysis was used to design variable contributions.

Based on the calculation dataset established by Table 5 of the SFE model, the experimental dataset obtained after solving the model is divided into two parts: training dataset and testing dataset. The training dataset is used to train the ANFIS-SHAMODE-IWOA model, and the testing dataset is used to test the performance of the ANFIS-SHAMODE-IWOA model. In order to eliminate the influence of sample selection on model training, a random sampling method is adopted to extract 70% of the dataset as the training dataset and 30% as the testing dataset. In addition, from Table 5, it can be observed that under different combinations of design parameters, the torque, torsion, total mass, and reliability index all undergo significant changes [40].

2) RELIABILITY ESTIMATION FOR ANFIS-SHAMODE-IWOA MODELS

In order to achieve accurate reliability estimation, optimize model performance, and effectively avoid ''dimension swallowing'', it is necessary to normalize all training and testing datasets to the range of (0, 1) before establishing the ANFIS model learned by the SHAMODE-IWOA algorithm using the training dataset. The normalization formula is shown as

TABLE 4. Table of SFE model parameters.

Variable	Description	Upper	Design Basis	Lower
V1	Longitudinal beam center outside	-2	0	2
V2	Fifth beam position	-1	0	1
V3	Sixth beam position	-1	0	1
V4	Height of the middle section of the longitudinal beam	-2	0	2
V5	Fourth beam cross-sectional area	-1	0	1
V6	Sixth beam cross-sectional area	-1	0	1
V7	Height of the middle section of the eighth beam	-1	0	1
V8	Width of section at both ends of the eighth beam	-1	0	1
V9	Thickness of outer plate of left longitudinal beam	2	3.2	4
V10	Reinforcing plate thickness after second section of outer plate of left stringer	2	2.8	4
V11	Left stringer inner plate middle section	2	3	4
V12	Left stringer inner plate rear segment	2	3	4
V13	Left stringer rear end first stiffener plate	2	3.2	4
V14	Left stringer rear end second stiffener plate	2	3.5	4
V15	Left stringer outer plate rear end	2	2.8	4
V16	Fourth beam top board	2	2.8	4
V17	Fourth beam under board	2	2.8	4
V18	Fifth beam on board	1.5	2	3
V19	Fifth beam under board	2	2.3	4
V20	Fifth beam under reinforcing plate	2	2.3	4
V21	Sixth beam lower board	2	3	4
V22	Seventh beam under board	2	2.3	4
V23	Seventh beam on board	2	2.3	4
V24	Eighth beam top board	2	2.3	4
V25	Eighth beam lower side left stiffener plate	2	2.8	4

TABLE 5. Table of SFE model parameters.

No	V1	V2	V3	V4	V5	V6	V7	V8	V9	V10	V11	V12	V13	V14	V15	V16	V17	V18	V19	V20	V21	V22	V23	V24	V25	Bending	Torsion	Mass	R
1	-2	-1	-1	-2	-1	-1	-1	-1	2	2	2	2	2	2	2	2	1.5	2	2	2	2	2	2	2	2	4510.77	230.69	0.20327	0.884
2	-2	-1	-1	-2	-1	-1	-1	-1	2	2	2	2	3.5	2.8	2.8	2.8	2	2.3	2.3	3	2.3	2.3	2.3	2.8	3.2	4387.71	206.66	0.18937	0.791
3	-2	-1	-1	-2	-1	-1	-1	-1	2	2	2	2	4	4	4	4	4	4	4	4	4	4	4	4	4	4268.21	196.44	0.18488	0.813
4	0	0	0	0	0	0	0	0	2.8	3	3	3.2	2	2	2	2	1.5	2	2	2	2	2	2	2	3.2	4124.91	194.93	0.1859	0.802
5	0	0	0	0	0	0	0	0	2.8	3	3	3.2	3.5	2.8	2.8	2.8	2	2.3	2.3	3	2.3	2.3	2.3	2.8	4	4530.42	193.54	0.1841	0.915
6	0	0	0	0	0	0	0	0	2.8	3	3	3.2	4	4	4	4	4	4	4	4	4	4	4	4	2	4322.35	192.08	0.1832	0.816
...																	.....												
100	2	1	1	2	1	1	1	1	4	4	4	4	2	2	2	2	1.5	2	2.3	3	2.3	2.3	2.3	2.8	2	4519.82	227.561	0.2472	0.913

follows (21):

$$\breve{x}_i(k) = \frac{x_i - x_{imin}}{x_{imax} - x_{imin}} \tag{21}$$

In formula (21), x_i, x_{imin} and x_{imax} are the original values, minimum values, and maximum values of the dataset, respectively; $\breve{x}_i(k)$ represents the k-th normalized value of the dataset.

After establishing the ANFIS-SHAMODE-IWOA model, the performance of the model is validated using the testing dataset. To quantify the performance of the ANFIS-SHAMODE-IWOA model, the R2 value, estimation accuracy (θ), and mean square error (MSE) are compared. The calculation methods are as follows:

$$R^2 = 1 - \frac{(M_t - P_t)^2}{\sum_{t=1}^{n}(M_t - \bar{M}_t)^2} \tag{22}$$

$$\theta = \left[1 - \left(\frac{1}{n}\sum_{t=1}^{n}\left|\frac{P_t - M_t}{M_t}\right|\right)\right] * 100\% \tag{23}$$

$$\mathrm{MSE} = \frac{1}{n}\sum_{t=1}^{n}(\bar{M}_t - P_t)^2 \tag{24}$$

In formula (22)(23)(24), M_t and P_t are the calculated reliability indexes and model estimates at the t-th iteration, n is the data quantity, and $\bar{M}_t$ is the average value of the calculated data.

The estimated results obtained from the ANFIS-SHAMODE-IWOA model using the testing dataset are shown in Figure 7 and Figure 8. In Figure 7, the reliability results calculated by the model are close to the estimated results. The maximum error between the calculated values and the estimated values is 9.6%, which is better than the accuracy results reported in related literature [41], [42]. The quantified test results show that the estimation accuracy θ, R^2, and MSE are 88.84%, 0.88172, and 0.0087, respectively. The scatter plot shown in Figure 8 indicates that the measured values and estimated values are evenly distributed on both sides of the line and exhibit the same trend. The results indicate that the model has good predictive estimation performance and can accurately estimate the structural reliability based on structural dimensions and shape parameters [43].

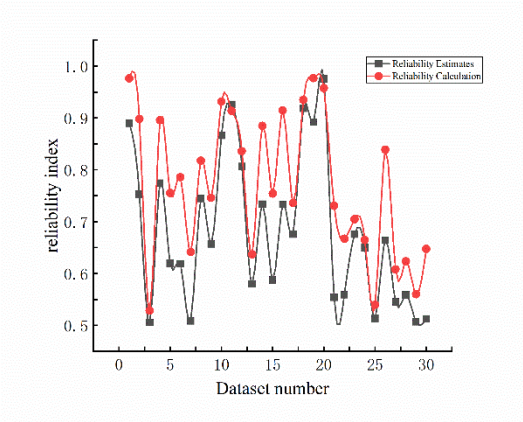

FIGURE 7. ANFIS-SHAMODE-IWOA model measurements and estimates.

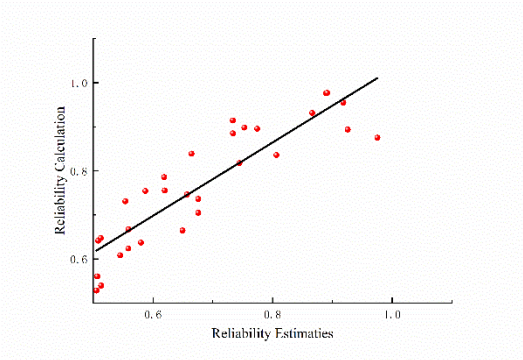

FIGURE 8. Scatter plot between the estimated and calculated reliability indices.

3) COMPARISON WITH OTHER MODELS

To clarify the superiority of ANFIS-SHAMODE-IWOA model, The ANFIS model based on particle swarm Optimization (PSO) learning (ANFIS-PSO) [44], ANFIS model based on genetic algorithm (ANFIS-GA) learning (47], ANFIS [30], Support Vector Machine (SVR) and Artificial Neural Network (ANN) model are compared respectively. The comparison results are shown in Table 6 below.

During the experiment, the trial-and-error method was used to determine the hyper parameters of the aforementioned model. Table 7 presents the comparative results of MAPE, MSE, and R2 in this study. The results show that the ANFIS-SHAMODE-IWOA model has the best estimation

TABLE 6. The model statistics calculate the comparison results.

Model	Statistical index		
	θ(%)	MSE	R^2
ANFIS-SHAMODE-IWOA	**88.84%**	**0.0087**	**0.88172**
ANFIS-PSO	81.45	0.0103	0.8163
ANFIS-GA	80.12%	0.0093	0.8046
ANFIS	78.49%	0.0117	0.7748
SVR	75.64%	0.0164	0.7639
ANN	74.33%	0.0176	0.7414

performance for truss reliability, with an R2 of 0.88172, MSE of 0.0087, and θ of 88.84%. Compared with the ANFIS-PSO, ANFIS-GA, and ANFIS models, the estimation performance of the ANFIS-SHAMODE-IWOA model has significantly improved.

The numerical results of the experiments demonstrate the excellent global convergence capability of the SHAMODE-IWOA algorithm, providing optimal premise and consequent parameters for the ANFIS model and enhancing the predictive ability of the ANFIS-SHAMODE-IWOA model. Compared with the ANFIS-PSO and ANFIS-GA models, the θ value of the ANFIS-SHAMODE-IWOA model has increased by 7.39% and 8.72%, respectively.

V. CHASSIS TRUSS STRUCTURE MULTI-OBJECTIVE OPTIMIZATION

Based on the above research and analysis, aiming at the data results in the table above and the reliability prediction model, this section intends to construct a multi-objective equation with the minimum quality and reliability measurement functions as objectives, with the fault probability as a constraint. The proposed SHAMODE-IWOA algorithm is then applied to solve it, and the solution results are verified through finite element and actual stress acquisition experiments.

A. ESTABLISHMENT OF MULTI-OBJECTIVE OPTIMIZATION EQUATION

The truss reliability and quality multi-objective equation can be formulated as follows [1]:

$$\begin{cases} \min\limits_{x} \{f_1(x,y); f_2(x,y)\} \\ S.TP_r \le 0.01 \end{cases} \tag{25}$$

In formula (25), P_r is the fault probability, x is the design variable vector, y is the physical vector containing yield strength, torsional stiffness, and applied loads, f_1 represents structural quality, which is the sum of the product of topological unit quality and density, and f_2 represents the reliability measurement function: $f_2 = 1/\beta$, where β is the reliability coefficient.

The reliability coefficient (β) refers to the shortest distance between the limit state line and the origin of the transformation space. A larger β indicates higher reliability (greater safety), usually represented by the following formula:

$$\beta = \mu_M / \sigma_M \tag{26}$$

In formula (26), $\mu_{,M}$ characterizes the average force under the limit failure function state, and σ_M characterizes the variance of the mechanical change rate under the limit failure function state.

The limit state failure function can be represented by the literature [46]:

$$M = G(R, S) = R - S \begin{cases} > 0 \ safety \\ \le 0 \ failure \end{cases} \tag{27}$$

In function (27), R represents the resistance failure characterization coefficient, and S describes the impact factor of external factors on the resistance characterization coefficient R. Therefore, μm and σ_m can be described as [47]:

$$\mu_M \approx G\left(\mu_{S_Y}, \{\mu_{F_{ex,i}}\}\right) = \mu_{S_Y} - \sum_{i=1}^{N_F} \frac{k_i \mu_{F_{ex,i}}}{N_F} = \mu_{S_Y} - S_e \tag{28}$$

$$\sigma_M^2 \approx \left(\frac{\partial G}{\partial S_Y}\right)^2_{\mu_{S_Y}} + \sum_{i=1}^{N_F} \left(\left(\frac{\partial G}{\partial F_{ex,i}}\right)_{\mu_{F_{ex,i}}} \sigma_{F_{ex,i}}\right)^2 = \sigma_{S_Y}^2 + \sum_{i=1}^{N_F} \left(\frac{k_i \sigma_{F_{ex,i}}}{N_F}\right)^2 \tag{29}$$

$$k_i = \frac{S_e}{F_{ex,i}} \tag{30}$$

In formula (28)(29)(30), k_i is the ratio of stress occurring on each truss component to the i-th external load, S_e is the stress occurring on each component, $F_{ex,i}$ is the external applied load; S_Y is the yield strength, N_Y is the type of structural material, μ_{SY} is the average value of S_Y, μ Fex is the average value of the applied load. σ^2_{SY} and $\sigma^2_{Fex;i}$ are the variances of S_Y and $F_{ex,i}$, respectively.

In addition, $F_{ex,i}$ is represented by the following linear equation:

$$\{F_{ex,i}\} = [K_{ij}]\{u_i\} \tag{31}$$

In equation (31), $[K_{ij}]$ is the N× N stiffness matrix, $\{u_i\}$ is the N×1 node displacement vector, and N is the number of degrees of freedom of the finite element.

Se can also be expressed by the following linear equation:

$$\{S_e\} = [T][K_{ij}]^{-1}\{F_{ex,i}\} \tag{32}$$

Therefore, the limit state function can be expressed as:

$$\{M_e\} = S_Y - \{S_e\} = S_Y - [T][K_{ij}]^{-1}\{F_{ex,i}\} \tag{33}$$

Thus, for the reliability coefficient of a specific component (e), $\mu_{M,e}$ and $\sigma_{M,e}$ can be approximated as follows [1]:

$$\beta_e = \frac{\mu_{M,e}}{\sigma_{M,e}} \tag{34}$$

$$\mu_{M,e} = \mu_{S_Y} - [T][K_{ij}]^{-1}\{\mu_{F_{ex,i}}\} \tag{35}$$

$$\sigma_{M,e} = \sigma_{S_Y} + \sum_{i=1}^{N_F} \left(\frac{\frac{[T][K_{ij}]^{-1}\{\mu_{F_{ex,i}}\}}{\mu_{F_{ex,i}}} \sigma_{F_{ex,i}}}{N_F}\right) \tag{36}$$

Thus, P_r can be expressed as follows:

$$P_r = \Phi(-\beta) \tag{37}$$

B. ESTABLISHMENT OF MULTI-OBJECTIVE OPTIMIZATION EQUATION

The SHAMODE-IWOA algorithm was used to optimize and solve the multi-objective function constructed in Section 3.3.2. The iterative solution results are shown in Figure 9:

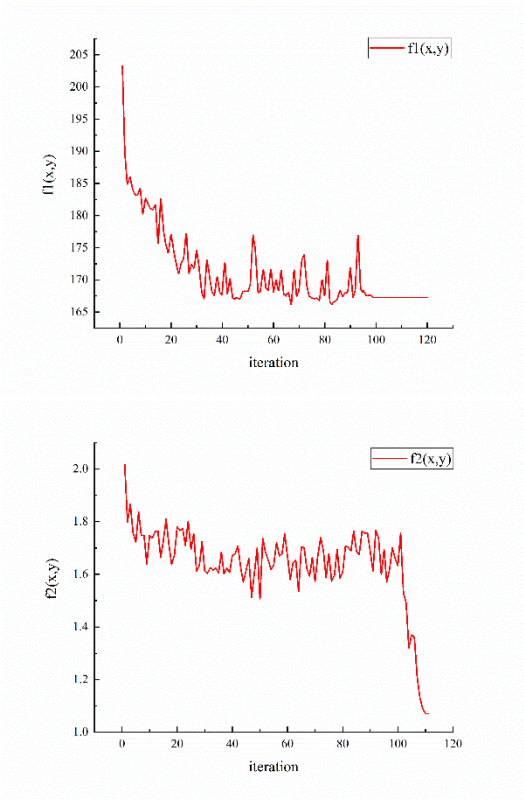

FIGURE 9. The graph of the iterative calculation result.

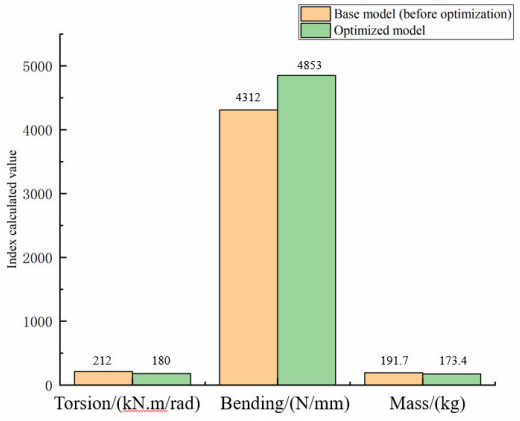

FIGURE 10. Design and calculate the comparison chart of optimization index.

Based on the iterative solution results mentioned above, the optimized values of design indicators were obtained using the "compromise method" as shown in Table 7. The calculated performance of the model after optimization is shown in Figure 10. According to the results shown in Figure 10, compared to the performance of the model before optimization, the optimized model shows a 15% decrease in the Torsion indicator, a 12.5% improvement in the Bending indicator, and a 9.5% improvement in the Mass indicator.

TABLE 7. The comparison results design value after optimization solution.

Design Parameter	V1	V2	V3	V4	V5
Post-optimized Value	-1.76	0.75	-0.26	0.84	0.63
Design Parameter	V6	V7	V8	V9	V10
Post-optimized Value	0.89	-0.63	2.41	2.12	2.80
Design Parameter	V11	V12	V13	V14	V15
Post-optimized Value	2.20	2	2	2	2
Design Parameter	V16	V17	V18	V19	V20
Post-optimized Value	2	2.7	1.5	2.4	2.5
Design Parameter	V21	V22	V23	V24	V25
Post-optimized Value	2	2	2	2	2

Further simulation calculations were performed on the finite element model constructed in Figure 5. Seven working conditions, including Back Acc, Back Brake1.0g, Brake1.2g, Bump3.5g, Cornering1.2g, Cornering Brake 0.74g, and Frot Acc, were selected for comparative analysis using finite element simulation. The optimized simulation results are shown in Figure 11, and the comparison between the optimized and original simulation results is shown in Table 8.

TABLE 8. Comparison table of FEM simulation calculation structures before and after optimization.

Working Condition	Basic Model (MPa)	Post-optimized Model (MPa)	Promotion
Back Acc	408.1	408	0.02%
Back Brake1.0g	308.2	290	5.9%
Brake1.2g	529.8	530	0.04%
Bump3.5g	623.4	620	0.55%
Cornering1.2g	436.4	436	0.09%
Cornering Brake 0.74g	464.4	464	0.09%
Frot Acc	299.7	298	0.57%

The optimized chassis frame had improved performance in all indicators while maintaining a certain degree of reduction in weight, with the Back Brake1.0g condition showing the largest improvement and an increase of 5.9%.

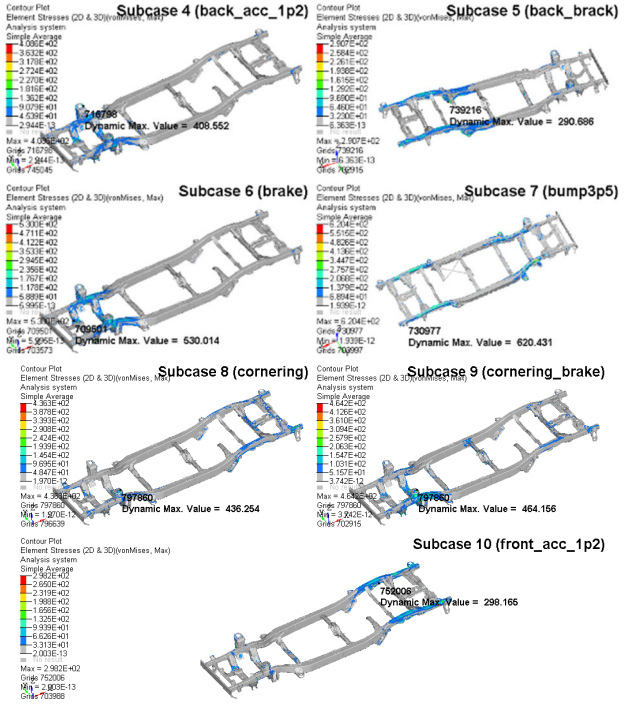

FIGURE 11. Results of truss finite element calculation after optimization.

To further verify the optimization results, strain tests were conducted on 25 key locations of the optimized chassis frame using electrical measurement. Local photos of the test are shown in Figure 12.

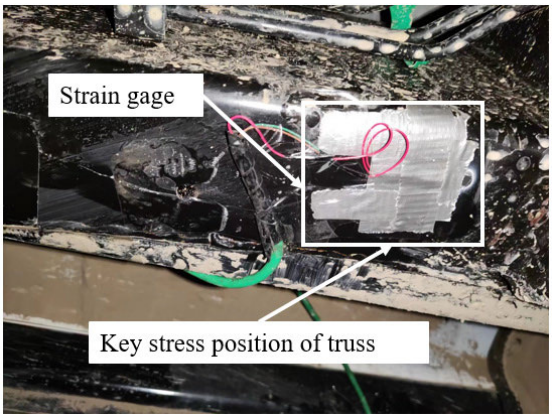

FIGURE 12. Stress test photo.

The vehicle equipped with the optimized chassis frame was subjected to 10 groups of 20 cycles of driving on typical harsh road surfaces, and data from the four groups with the highest stress values in the test cycles are presented in Figure 13 [48], [49].

The stress data were separated according to the rain-flow counting method, and the corresponding damage coupling values were calculated for each stress level at the four positions as listed in Table 9. Based on the Weibull distribution model for lifetime probability [50], the comprehensive

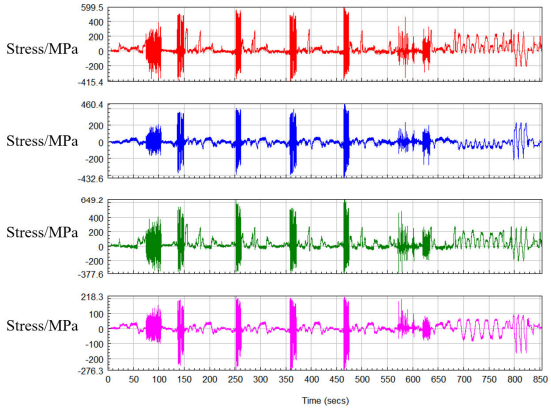

FIGURE 13. Map of stress acquisition test results.

TABLE 9. Results of damage coupling value calculation.

Stress Level (MPa)	Stress Amplitude/S_a	Stress Mean/S_m	Cycle/n_i	Damage/ ($1/N_i$)	Total Damage/ (n_i/N_i)
Level 1	631.717	206.43	1	3.162×10^{-6}	3.162×10^{-6}
Level 2	529.301	206.43	12	1.843×10^{-6}	2.211×10^{-5}
Level 3	476.802	206.43	43	7.903×10^{-7}	3.398×10^{-5}
Level 4	318.69	206.43	117	2.764×10^{-7}	3.233×10^{-5}
Level 5	253.241	206.43	453	1.219×10^{-7}	5.522×10^{-5}
Level 6	198.462	206.43	3007	1.842×10^{-8}	5.538×10^{-5}
Level 7	169.107	206.43	10361	1.198×10^{-9}	1.241×10^{-5}
Level 8	89.50	206.43	20153	7.437×10^{-11}	1.499×10^{-6}
Level 9	43.77	206.43	145740	3.028×10^{-12}	4.413×10^{-7}

reliability index was calculated to be 0.9317, which meets the requirements for structural reliability and is close to the optimized calculation value.

In summary, this section used the proposed SHAMODE-IWOA algorithm to optimize the chassis frame structure of a certain brand of dump truck. After adjusting the relevant design parameters based on the optimized calculation results, the chassis frame was manufactured and tested through mathematical model calculation, finite element simulation, and stress actual testing. The test results showed that the optimized chassis frame structure had improved performance in torsion, bending, and mechanical properties while reducing the total weight and improving reliability, demonstrating good engineering application value for the algorithm.

VI. CONCLUSION

The design of self-dumping truck chassis frame structure with consideration of both quality and reliability indicators is a

challenging and difficult task for designers. To unleash the potential performance of the chassis and improve the efficiency of design work, this paper proposes a multi-objective optimization design system for the reliability estimation and design parameter optimization of the chassis frame structure based on the SHAMODE-IWOA algorithm and ANFIS-SHAMODE-IWOA model. The specific conclusions are as follows:

(1) In response to the low solving efficiency and insufficient search capability of the SHAMODE algorithm, this paper introduces an adaptive spiral search strategy based on the SHAMODE-WO algorithm and proposes a new algorithm called SHAMODE-IWOA. Benchmark function experiments demonstrate that the SHAMODE-IWOA algorithm outperforms other similar products in 21 out of 30 benchmark functions, indicating better search and convergence performance.

(2) To accurately estimate the reliable durability performance of chassis truss structures, this paper optimizes the model parameters using the SHAMODE-IWOA algorithm based on the traditional ANFIS model. Experimental results show that the ANFIS-SHAMODE-IWOA model can accurately estimate the reliability of the chassis truss structure, with performance indicators MAPE, R2, and MSE reaching 6.5%, 0.954, and 0.006 respectively. Compared to the ANFIS-PSO, ANFIS-H, ANFIS-GA, ANN, and SVR models on the same dataset, the ANFIS-SHAMODE-IWOA model exhibits better estimation performance.

(3) To obtain the minimum mass and optimal reliable durability of chassis truss structures, it is necessary to find the optimal combination of design parameters. This paper uses the SHAMODE-IWOA algorithm to perform multi-objective optimization on the design parameters of truss structures. After optimization, the performance of the solved model is compared to the performance before optimization, showing a 15% decrease in the Torsion index, a 12.5% improvement in the Bending index, and a 9.5% improvement in the Mass index. Furthermore, subsequent finite element simulation and stress testing experiments validate its effectiveness.

However, the experimental results also indicate that there is still room for improvement in the convergence efficiency and solution quality of the SHAMODE-IWOA algorithm. Additionally, when dealing with higher-dimensional and complex engineering design problems such as composite parts, elastic components, rubber products, and complex structural components, further research and exploration are needed to study its global optimization behavior and predictive capabilities in more depth.

ACKNOWLEDGMENT

Zhao Minqing would like thank Prof. Wang Hongxi from the School of Mechanical and Electrical Engineering, Xi'an Technological University, for his unwavering support of this research. His invaluable insights and scientific methodology have greatly contributed to the development of this study. He also would like to thank Doctoral student Chen Weihuan from East China Jiaotong University for his meticulous review of the language and presentation of this article, which has significantly improved its quality, also would like to thank Prof. Ning Shanping from Xi'an Technological University for providing the necessary facilities and resources for the execution of this research, and also would like to thank their support and expertise have been instrumental in the successful completion of this work. The completion of this article would not have been possible without the generous support and guidance of several individuals to whom he owe his deepest gratitude.

AVAILABILITY OF DATA AND MATERIAL

The code in this article can be found in the following links: https://gitee.com/zhao-minqing/matlab.

REFERENCES

[1] N. Panagant, S. Bureerat, and K. Tai, "A novel self-adaptive hybrid multi-objective meta-heuristic for reliability design of trusses with simultaneous topology, shape and sizing optimisation design variables," *Structural Multidisciplinary Optim.*, vol. 60, no. 5, pp. 1937–1955, Jun. 2019, doi: 10.1007/s00158-019-02302-x.

[2] P. Hajela and E. Lee, "Genetic algorithms in truss topological optimization," *Int. J. Solids Struct.*, vol. 32, no. 22, pp. 3341–3357, Nov. 1995, doi: 10.1016/0020-7683(94)00306-H.

[3] M. Ohsaki, "Genetic algorithm for topology optimization of trusses," *Comput. Struct.*, vol. 57, no. 2, pp. 215–219, 1995, doi: 10.1016/0045-7949(94)00617-C.

[4] G.-S. Chen, R. J. Bruno, and M. Salama, "Optimal placement of active/passive members in truss structures using simulated annealing," *AIAA J.*, vol. 29, no. 8, pp. 1327–1334, Aug. 1991, doi: 10.2514/3.10739.

[5] J. F. Schutte and A. A. Groenwold, "Sizing design of truss structures using particle swarms," *Struct. Multidisciplinary Optim.*, vol. 25, no. 4, pp. 261–269, 2003, doi: 10.1007/s00158-003-0316-5.

[6] N. Panagant, N. Pholdee, S. Bureerat, A. R. Yildiz, and S. Mirjalili, "A comparative study of recent multi-objective metaheuristics for solving constrained truss optimisation problems," *Arch. Comput. Methods Eng.*, vol. 28, no. 5, pp. 4031–4047, Aug. 2021, doi: 10.1007/s11831-021-09531-8.

[7] S. Kumar, P. Jangir, G. G. Tejani, M. Premkumar, and H. H. Alhelou, "MOPGO: A new physics-based multi-objective plasma generation optimizer for solving structural optimization problems," *IEEE Access*, vol. 9, pp. 84982–85016, 2021, doi: 10.1109/ACCESS.2021.3087739.

[8] S. Anosri, N. Panagant, P. Champasak, S. Bureerat, C. Thipyopas, S. Kumar, N. Pholdee, B. S. Yıldız, and A. R. Yildiz, "A comparative study of state-of-the-art metaheuristics for solving many-objective optimization problems of fixed wing unmanned aerial vehicle conceptual design," *Arch. Comput. Methods Eng.*, vol. 30, no. 6, pp. 3657–3671, Jul. 2023, doi: 10.1007/s11831-023-09914-z.

[9] Z. Meng, B. S. Yıldız, G. Li, C. Zhong, S. Mirjalili, and A. R. Yildiz, "Application of state-of-the-art multiobjective metaheuristic algorithms in reliability-based design optimization: A comparative study," *Structural Multidisciplinary Optim.*, vol. 66, no. 8, p. 191, Aug. 2023, doi: 10.1007/s00158-023-03639-0.

[10] B. Zhan and W. Gu, "A multi-stage adaptive sequential parameter exploration hunger games search algorithm for solving complex optimization problems," *IEEE Access*, vol. 11, pp. 100919–100947, 2023, doi: 10.1109/ACCESS.2023.3308690.

[11] T. Kunakote, N. Sabangban, S. Kumar, G. G. Tejani, N. Panagant, N. Pholdee, S. Bureerat, and A. R. Yildiz, "Comparative performance of twelve metaheuristics for wind farm layout optimisation," *Arch. Comput. Methods Eng.*, vol. 29, no. 1, pp. 717–730, Jan. 2022, doi: 10.1007/s11831-021-09586-7.

[12] B. S. Yıldız, S. Kumar, N. Pholdee, S. Bureerat, S. M. Sait, and A. R. Yildiz, "A new chaotic Lévy flight distribution optimization algorithm for solving constrained engineering problems," *Exp. Syst.*, vol. 39, no. 8, Sep. 2022, Art. no. e12992, doi: 10.1111/exsy.12992.

[13] S. M. Sait, P. Mehta, D. Gürses, and A. R. Yildiz, "Cheetah optimization algorithm for optimum design of heat exchangers," *Mater. Test.*, vol. 65, no. 8, pp. 1230–1236, Aug. 2023, doi: 10.1515/mt-2023-0015.

[14] B. S. Yıldız, N. Pholdee, N. Panagant, S. Bureerat, A. R. Yildiz, and S. M. Sait, "A novel chaotic Henry gas solubility optimization algorithm for solving real-world engineering problems," *Eng. Comput.*, vol. 38, no. S2, pp. 871–883, Jun. 2022, doi: 10.1007/s00366-020-01268-5.

[15] D. Greiner, J. Periaux, J. M. Emperador, B. Galván, and G. Winter, "Game theory based evolutionary algorithms: A review with Nash applications in structural engineering optimization problems," *Arch. Comput. Methods Eng.*, vol. 24, no. 4, pp. 703–750, Nov. 2017, doi: 10.1007/s11831-016-9187-y.

[16] Z. Tang, X. Hu, and J. Périaux, "Multi-level hybridized optimization methods coupling local search deterministic and global search evolutionary algorithms," *Arch. Comput. Methods Eng.*, vol. 27, pp. 939–975, Mar. 2019, doi: 10.1007/s11831-019-09336-w.

[17] B. Aslan and A. R. Yıldız, "Optimum design of automobile components using lattice structures for additive manufacturing," *Mater. Test.*, vol. 62, no. 6, pp. 633–639, Jun. 2020, doi: 10.3139/120.111527.

[18] S. Kumar, P. Jangir, G. G. Tejani, and M. Premkumar, "A decomposition based multi-objective heat transfer search algorithm for structure optimization," *Knowl.-Based Syst.*, vol. 253, Oct. 2022, Art. no. 109591, doi: 10.1016/j.knosys.2022.109591.

[19] P. Mehta, B. S. Yildiz, S. M. Sait, and A. R. Yildiz, "Hunger games search algorithm for global optimization of engineering design problems," *Mater. Test.*, vol. 64, no. 4, pp. 524–532, Apr. 2022, doi: 10.1515/mt-2022-0013.

[20] S. Kumar, N. Panagant, G. G. Tejani, N. Pholdee, S. Bureerat, N. Mashru, and P. Patel, "A two-archive multi-objective multi-verse optimizer for truss design," *Knowl.-Based Syst.*, vol. 270, Jun. 2023, Art. no. 110529, doi: 10.1016/j.knosys.2023.110529.

[21] K. Zhao, P. Wang, and X. Tong, "An adaptive two-population evolutionary algorithm for constrained multi-objective optimization problems," *IEEE Access*, vol. 11, pp. 82118–82131, 2023, doi: 10.1109/ACCESS.2023.3300590.

[22] P. Mehta, B. S. Yıldız, S. M. Sait, and A. R. Yıldız, "Gradient-based optimizer for economic optimization of engineering problems," *Mater. Test.*, vol. 64, no. 5, pp. 690–696, May 2022, doi: 10.1515/mt-2022-0055.

[23] A. Nonut, Y. Kanokmedhakul, S. Bureerat, S. Kumar, G. G. Tejani, P. Artrit, A. R. Yıldız, and N. Pholdee, "A small fixed-wing UAV system identification using metaheuristics," *Cogent Eng.*, vol. 9, no. 1, Dec. 2022, Art. no. 2114196, doi: 10.1080/23311916.2022.2114196.

[24] N. Panagant, S. Kumar, G. G. Tejani, N. Pholdee, and S. Bureerat, "Many-objective meta-heuristic methods for solving constrained truss optimisation problems: A comparative analysis," *MethodsX*, vol. 10, 2023, Art. no. 102181, doi: 10.1016/j.mex.2023.102181.

[25] S. Bureerat and K. Sriworamas, "Simultaneous topology and sizing optimization of a water distribution network using a hybrid multiobjective evolutionary algorithm," *Appl. Soft Comput.*, vol. 13, no. 8, pp. 3693–3702, Aug. 2013, doi: 10.1016/j.asoc.2013.04.005.

[26] S. Bureerat and K. Sriworamas, "Population-based incremental learning for multi-objective optimisation," in *Soft Computing in Industrial Applications*. Berlin, Germany: Springer, 2007, pp. 223–232.

[27] R. Tanabe and A. S. Fukunaga, "Improving the search performance of SHADE using linear population size reduction," in *Proc. IEEE Congr. Evol. Comput. (CEC)*, Jul. 2014, pp. 1658–1665.

[28] S. Anosri, N. Panagant, S. Bureerat, and N. Pholdee, "Success history based adaptive multi-objective differential evolution variants with an interval scheme for solving simultaneous topology, shape and sizing truss reliability optimisation," *Knowl.-Based Syst.*, vol. 253, Oct. 2022, Art. no. 109533, doi: 10.1016/j.knosys.2022.109533.

[29] S. Mirjalili and A. Lewis, "The whale optimization algorithm," *Adv. Eng. Softw.*, vol. 95, pp. 51–67, May 2016, doi: 10.1016/j.advengsoft.2016.01.008.

[30] K. Mohammadi, S. Shamshirband, D. Petković, P. L. Yee, and Z. Mansor, "Using ANFIS for selection of more relevant parameters to predict dew point temperature," *Appl. Thermal Eng.*, vol. 96, pp. 311–319, Mar. 2016, doi: 10.1016/j.applthermaleng.2015.11.081.

[31] A. LaTorre and J.-M. Peña, "A comparison of three large-scale global optimizers on the CEC 2017 single objective real parameter numerical optimization benchmark," in *Proc. IEEE Congr. Evol. Comput. (CEC)*, Jun. 2017, pp. 1063–1070.

[32] M. Tubishat, M. A. M. Abushariah, N. Idris, and I. Aljarah, "Improved whale optimization algorithm for feature selection in Arabic sentiment analysis," *Int. J. Speech Technol.*, vol. 49, no. 5, pp. 1688–1707, May 2019, doi: 10.1007/s10489-018-1334-8.

[33] G. Kaur and S. Arora, "Chaotic whale optimization algorithm," *J. Comput. Design Eng.*, vol. 5, no. 3, pp. 275–284, Jul. 2018, doi: 10.1016/j.jcde.2017.12.006.

[34] D. Gürses, P. Mehta, S. M. Sait, and A. R. Yildiz, "African vultures optimization algorithm for optimization of shell and tube heat exchangers," *Mater. Test.*, vol. 64, no. 8, pp. 1234–1241, Aug. 2022, doi: 10.1515/mt-2022-0050.

[35] D. Gürses, P. Mehta, V. Patel, S. M. Sait, and A. R. Yildiz, "Artificial gorilla troops algorithm for the optimization of a fine plate heat exchanger," *Mater. Test.*, vol. 64, no. 9, pp. 1325–1331, Sep. 2022, doi: 10.1515/mt-2022-0049.

[36] J. Xue and B. Shen, "Dung beetle optimizer: A new meta-heuristic algorithm for global optimization," *J. Supercomput.*, vol. 79, no. 7, pp. 7305–7336, May 2023, doi: 10.1007/s11227-022-04959-6.

[37] F. A. Hashim and A. G. Hussien, "Snake optimizer: A novel meta-heuristic optimization algorithm," *Knowl.-Based Syst.*, vol. 242, Apr. 2022, Art. no. 108320, doi: 10.1016/j.knosys.2022.108320.

[38] C. Yu, M. Chen, K. Cheng, X. Zhao, C. Ma, F. Kuang, and H. Chen, "SGOA: Annealing-behaved grasshopper optimizer for global tasks," *Eng. Comput.*, vol. 38, no. S5, pp. 3761–3788, Dec. 2022, doi: 10.1007/s00366-020-01234-1.

[39] Z. Xin, J. Zhang, Y. Jin, J. Zheng, and Q. Liu, "Predicting the alloying element yield in a ladle furnace using principal component analysis and deep neural network," *Int. J. Minerals, Metall. Mater.*, vol. 30, no. 2, pp. 335–344, Feb. 2023.

[40] Y. Wang, Z. Zhu, A. Sha, and W. Hao, "Low cycle fatigue life prediction of titanium alloy using genetic algorithm-optimized BP artificial neural network," *Int. J. Fatigue*, vol. 172, Jul. 2023, Art. no. 107609, doi: 10.1016/j.ijfatigue.2023.107609.

[41] L. Ye, W. Zhang, Y. Cui, and S. Deng, "Dynamic evaluation of the degradation process of vibration performance for machine tool spindle bearings," *Sensors*, vol. 23, no. 11, p. 5325, Jun. 2023, doi: 10.3390/s23115325.

[42] L. Xu, C. Huang, C. Li, J. Wang, H. Liu, and X. Wang, "Estimation of tool wear and optimization of cutting parameters based on novel ANFIS-PSO method toward intelligent machining," *J. Intell. Manuf.*, vol. 32, no. 1, pp. 77–90, Jan. 2021, doi: 10.1007/s10845-020-01559-0.

[43] Y. S. Kong, S. Abdullah, D. Schramm, M. Z. Omar, and S. M. Haris, "Design of artificial neural network using particle swarm optimisation for automotive spring durability," *J. Mech. Sci. Technol.*, vol. 33, no. 11, pp. 5137–5145, Nov. 2019, doi: 10.1007/s12206-019-1003-9.

[44] M. H. Djavareshkian and A. Esmaeili, "Heuristic optimization of submerged hydrofoil using ANFIS–PSO," *Ocean Eng.*, vol. 92, pp. 55–63, Dec. 2014, doi: 10.1016/j.oceaneng.2014.09.033.

[45] S. Vafaei, A. Rezvani, M. Gandomkar, and M. Izadbakhsh, "Enhancement of grid-connected photovoltaic system using ANFIS-GA under different circumstances," *Frontiers Energy*, vol. 9, no. 3, pp. 322–334, Sep. 2015.

[46] D. Greiner and P. Hajela, "Truss topology optimization for mass and reliability considerations—Co-evolutionary multiobjective formulations," *Structural Multidisciplinary Optim.*, vol. 45, no. 4, pp. 589–613, Apr. 2012, doi: 10.1007/s00158-011-0709-9.

[47] C. A. Cornell, "A probability-based structural code," *J. Amer. Concrete Inst.*, vol. 66, no. 12, pp. 974–985, 1969, doi: 10.14359/7446.

[48] W. Huang, "The frequency domain estimate of fatigue damage of combined load effects based on the rain-flow counting," *Mar. Struct.*, vol. 52, pp. 34–49, Mar. 2017, doi: 10.1016/j.marstruc.2016.11.004.

[49] Y. Liu, F. J. H. G. Kessels, W. D. van Driel, J. A. S. van Driel, F. L. Sun, and G. Q. Zhang, "Comparing drop impact test method using strain gauge measurements," *Microelectron. Rel.*, vol. 49, nos. 9–11, pp. 1299–1303, Sep. 2009, doi: 10.1016/j.microrel.2009.07.008.
[50] J. D. Baldwin and J. G. Thacker, "A starin-based fatigue reliability analysis method," *J. Mech.*, vol. 117, no. 2, pp. 229–234, 1995.

ZHAO MINQING was born in Jiangxi. He received the M.S. degree in mechanical engineering from Nanchang Hangkong University, in 2022. He is currently pursuing the Ph.D. degree with Xi'an Technological University. His research interests include optimization design algorithms and stress fatigue analysis.

WANG HONGXI received the Ph.D. degree from Xidian University, in 2006. He is currently working in Xi'an, Shaanxi, China. He is also a Professor with Xi'an Technological University. His main research interests include ultra-precision measurement theory and instrument design, intelligent sensors, and flexible mechanism design theory and application.

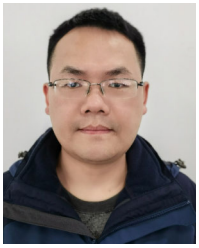

CHEN WEIHUAN received the master's degree in vehicle engineering from Shenyang Jianzhu University, in 2012. He is currently pursuing the Ph.D. degree with the School of Information Engineering, East China Jiaotong University. He is also an Intermediate Engineer with JMC & Ford. His research interests include artificial intelligence computing and computer simulation computing.

NING SHANPING was born in Guangzhou, China. He received the master's degree in mechanical design and theory from Jiangsu University of Science and Technology. He is currently pursuing the Ph.D. degree in mechanical design and automation with the School of Mechanical and Electrical Engineering, Xi'an Technological University. He is also a Senior Lecturer with the School of Rail Transit, Guangdong Transportation Vocational College. He has led several provincial-level research projects, contributed to the writing of three publications, and textbooks. He is also focused on research in the fields of target detection technology and machine learning.